Theoretical study of long-lived mode in tokamaks

Weichao Xie (谢维超)
Southwestern Institute of Physics, Chengdu, China, 610041

Long-lived mode (LLM) in rotating plasmas is studied by using a alternative dispersion relation. This work offers a theoretical interpretation of LLM observed in experiments [Heidbrink, Phys. Rev. Lett. **57**, 835 (1986); Chapman, Nucl. Fusion **50**, 045007 (2010)]. It is found that in rotating plasmas, LLM can transform from the fishbone mode. The real frequency of LLM, independent of the characteristic frequency of energetic ions (EIs), is proportional to the on-axis rotation frequency of bulk plasma. The key conditions to cause transition between the fishbone mode and LLM are weak magnetic shear (for both monotonic and nonmonotonic safety factor profile) and plasma rotation. The fishbone mode can evolve into LLM only when rotating speed is bigger than a critical value in low shear plasmas. The critical beta of EIs to induce LLM is very low. LLM is nonresonantly excited by EIs, and the driving sources mainly come from plasma inertia.

I. INTRODUCTION

The fishbone (FB) mode, energetic particles (EPs) excitation of internal kink mode with mode number $n = 1$ via resonance, was first observed in PDX neutral-beam injection (NBI) experiment [1]. Subsequently, the FB mode was successfully explained by the drift kinetic theory of EPs [2–4]. Besides FB mode, another branch of low frequency mode, the magnetic perturbation behaving long lasting saturated ideal internal kink instability [5–11], first observed during tangential NBI heated plasmas in PBX tokamak [5], has frequency close to on-axis toroidal rotation frequency of bulk plasmas. In MAST NBI heated discharges, it was found that the $n = 1$ FB modes usually evolve into the long-lived mode (LLM), which can be observed in the plasmas with safety factor profile either weakly reversed shear or broad low-shear regions [6,7]. The results in HL-2A tokamak show that the FB mode can evolve into LLMs in the case of monotonic safety factor profile with weak magnetic shear in the core plasma region [12–14]. Experiments indicate that plasma rotation and weak magnetic shear in the core plasma regions play crucial role in causing the transition between FB mode and LLM [6–16]. Moreover, in comparison with FB instabilities driven by energetic particles, the critical beta to drive LLM is relatively low; thus it is easy for LLM to be excited by EPs [9].

It is well known that the resonant driving sources to excite FB instabilities mainly come from pressure gradient of EPs (i.e., ∇P_h). Therefore, redistributions of energetic ions, exerting an important influence on FB mode and LLM, tend to flatten the pressure profile of EIs in the central region [15,16], and FB mode may be not observed during LLM activity due to decreasing of ∇P_h. Experiments show that, during LLM activity, NBI ions are redistributed but not significantly lost [15,16]. Dramatically decreasing of EP lost during LLM activity maybe related to lack of resonance between energetic particles and perturbations, which is the necessary condition

for LLM to have long lasting saturation. Thus the resonant excitation source from ∇P_h is weakened; instead, the nonresonant excitation from plasma inertia is dominant, indicating that LLM, a branch of nonresonant MHD mode, may have zero frequency in static plasmas.

On many tokamaks, such as HL-2A, MAST and TCV, when FB mode evolves into LLM, the frequency depends on plasma rotation [5–10]. For instance, the results in HL-2A NBI heated experiments [9], where the frequency of LLM is 10.5 kHZ, are in exact agreement with the toroidal rotation frequency at the location of minor radius $r = 0.2$ cm (i.e., near the position of the magnetic axis, see Fig. 3 in Ref. [9]). Meanwhile the lines shown in Fig. 1(a) are a time evolution of the mode frequency (solid line) and on-axis toroidal rotation frequency (dashed line) in HL-2A shot 21787. Similar results were also observed in MAST neutral beam injection heated experiments. The lines shown in Fig. 1(b) are a temporal evolution of the mode frequency of LLM (solid line) and central plasma rotation frequency (dashed line) in MAST shot 21781 with major radius $R_0 = 0.9$ m between $t = 0.256$ s and 0.32 s [6–8]. It can be learnt from the experimental results in Fig. 1 that the frequency of LLM is in good agreement with toroidal rotation frequency of bulk plasmas near magnetic axis, implying that the real frequency of LLM is almost zero in static plasmas. The numerical simulation of the FB mode in static plasmas shows that the real frequency of the FB mode can evolve to a value being approximately close to zero [17]. In addition, the long-lived mode is also explained as a branch of a nonresonant FB mode excited by energetic ions but with a local interchangelike mode structure [18].

This paper is organized as follows. In Sec. II, the new dispersion relation to study the FB mode and the corresponding analytical results are given. The numerical results are presented in Sec. III, and the main results are summarized in Sec. IV.
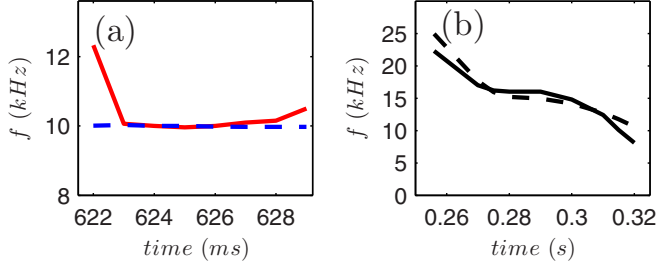
FIG. 1. Temporal evolution of mode frequency of LLM (solid line) and central toroidal rotation frequency (dashed line) in HL-2A discharge 21787 (a) and in MAST shot 21781 (b).

II. THE DISPERSION RELATION IN ROTATING PLASMAS

In rotating plasmas, the inertial term is modified by rotation due to the contribution of centrifugal force and Coriolis force. When both centrifugal and Coriolis forces are taken into account, the equation of motion in ideal plasmas can be written as [19]

$$\rho \frac{\partial \delta \vec{v}}{\partial t} = \delta \vec{J} \times \vec{B} + \vec{J} \times \delta \vec{B} - \nabla \delta p_c - \nabla \bullet \delta \overleftrightarrow{p}_h + \rho \vec{a}_c. \quad (1)$$

The last term on the RHS of Eq. (1) is the contribution from plasma rotation, and the expression $\vec{a}_c = 2\delta \vec{v} \times \vec{\Omega} - \delta \rho \vec{V}_0 \bullet \nabla \vec{V}_0 / \rho - \delta \vec{v} \bullet \nabla \vec{V}_0 - \vec{V}_0 \bullet \nabla \delta \vec{v}$ is the effective inertial force acceleration generated by Coriolis and centrifugal forces. The variables ρ and Ω are mass density of plasma and rotation frequency, respectively. The variable $\delta \vec{v}$ is perturbed velocity of plasmas, $\delta \rho = -\nabla \rho \cdot \xi$ is plasma perturbed density and V_0 is equilibrium flow. The first two terms and the third one on the RHS of Eq. (1) are current and bulk plasma pressure perturbations, respectively. The latter is $\delta p_c = -\xi \cdot \nabla P_{\text{eq}} - \Gamma P_{\text{eq}} \nabla \cdot \xi$ with Γ being the ratio of specific heat and P_{eq} being the equilibrium pressure of thermal particles. The fourth term on the RHS of Eq. (1) is the kinetic pressure of EIs, which is written as $\delta \overleftrightarrow{p}_h = \delta p_{h\perp} \overleftrightarrow{I} + (\delta p_{h//} - \delta p_{h\perp}) \vec{b}\vec{b}$. Here $\overleftrightarrow{I}$ is unit tensor and $\vec{b} = \vec{B}/|\vec{B}|$ is unit vector along equilibrium magnetic field. The perpendicular and parallel components of pressure $\delta p_{h\perp}$, $\delta p_{h//}$ are given in Refs. [2,20]. The radial profiles of rotation $\Omega(\hat{r})$ and plasma density $\rho(\hat{r})$ are, respectively, assumed to be $\Omega(r) = \Omega_0 g(r)$ and $\rho(r) = \rho_0 f(r)$ with $g(r) = [1 - [(r - r_{\Omega})/a]^2]^{\sigma_{\Omega}}$ and $f(r) = [1 - (r/a)^2]^{\sigma_{\rho}}$. Here, ρ_0 and Ω_0 are the values of $\Omega(0)$ and $\rho(0)$ and r_{Ω} is the peak position of rotation profile. The density profile of energetic ions is assumed to be $n_{0h}(r) \sim \exp[-\sigma^2(r - r_h)^2]$ and a slowing-down energy distribution of EIs is used [2,3]. The pitch angle distribution of EIs is $h(\alpha) \sim \exp[-(\alpha - \alpha_0)^2/\Delta^2]$ with pitch angle $\alpha = \mu B/E$ (μ is the magnetic moment and E is the energy of EIs). The variable Δ denotes the half width of pitch angle distribution and $\alpha_0 = \mu B_0/E$ is the peak position of $h(\alpha)$. A steplike trial function (i.e., the perturbed plasma displacement) inside $q = 1$ (or q_{min}) surface is used to establish the dispersion relation. Assuming circular cross sections, through straightforward manipulation of Eq. (1) in toroidal geometry (see the appendix), a dispersion relation

including both monotonic (positive shear) and nonmonotonic (negative shear) safety factor profile can be written as follows:

$$i\frac{\omega - \Omega_0}{\omega_A}\left[\left(\frac{\omega - \Omega_0}{\sqrt{2}\hat{s}\omega_A}\frac{\omega_+ - i\omega_-}{\omega_+\omega_-}\right)^l\left(1 + \frac{g_1\Omega_0}{\omega - \Omega_0}\right)\right.$$
$$\left. + i\frac{\Omega_0}{\hat{s}^2\omega_A}\left(C_1 + \frac{C_2\Omega_0}{\omega - \Omega_0}\right)\right]f_1 = \delta\hat{W}_c + \delta\hat{W}_k, \quad (2)$$

$$\delta\hat{W}_k = \frac{\beta_h R}{2r_s I}\int_{\sqrt{\alpha_1}}^{\sqrt{\alpha_2}}h(\alpha^2)d\alpha\int_{\hat{r}_1}^1\hat{r}d\hat{r}\frac{dn_{0h}}{d\hat{r}}KK_2$$
$$\times\left[1 - \frac{K_2}{qK_c}\left(1 + \frac{(\omega - \Omega_0)\hat{r}}{qK_c\omega_{ds}}\ln\left(1 - \frac{qK_c\omega_{ds}}{(\omega - \Omega_0)\hat{r}}\right)\right)\right], \quad (3)$$

$$\delta\hat{W}_c = 3\pi(1 - q_{0/\text{min}})\varepsilon^2(13/144 - \beta_{ps}^2), \quad (4)$$

where the normalized minor radius $\hat{r} = r/r_s$, and r_s is the position of inertial layer. The integer l set to be $l = 0$ and $l = 1$ denotes the case of monotonic safety factor profile (i.e., positive magnetic shear) and a nonmonotonic one but with q_{min} slightly bigger than unity (i.e., negative magnetic shear), respectively. For the former, the magnetic shear at the location of inertial layer is $\hat{s} = r_s q'_s$ while for the latter, the magnetic shear at the q_{min} position is $\hat{s} = r_s^2 q''_s$ instead of depending on dq/dr thanks to the derivatives of safety factor profile at this position is zero. The safety factor profiles in the case of monotonic and nonmonotonic distribution are assumed to be, respectively,

$$q = q_0 + (1 - q_0)\hat{r}^2, \quad (5)$$

$$q = q_{\text{min}} + \alpha_q(1 - \hat{r}^2)^2, \quad (6)$$

for the monotonic q profile in Eq. (5), $q_0 = q(0)$ represents the safety factor value on the magnetic axis whereas for the nonmonotonic q profile in Eq. (6), q_{min} denotes a minimum safety factor value at r_s where $q'(r_s) = 0$ and $\delta q = q(r_s) - 1 \ll 1$ which causes q_{min} to be slightly above 1. α_q is a constant to describe the shear of q profile. $\omega_{\pm} = \sqrt{\frac{\omega - \Omega_0}{\omega_A} \pm r_s^2 q''\delta q}$, $\beta_{ps} = -(\frac{R_0}{r_s})^2\beta_0(C_p + C_{\Omega}\frac{2\Omega_0^2 R_0 a}{\beta_0 V_A^2})$, $I = \int_{\sqrt{\alpha_1}}^{\sqrt{\alpha_2}}h(\alpha^2)d\alpha\int_{\hat{r}_1}^1 Kn_{0h}\hat{r}d\hat{r}$, $\beta = \frac{2\mu_0 p}{B^2}$ is a beta of plasmas with $\beta_0 = \beta(0)$, Eq. (4) is given in Ref. [21]. $\varepsilon = r_s/R_0$ is the inverse aspect ratio and R_0 is the major radius. β_h is the beta of EIs, $K_2 = 2E/K - 1$ (K and E are the complete elliptic integrals). $K_c = 2E/K - 1 + 4s(E/K - 1 + k^2)$ with argument $k^2 = (1/\alpha - 1 + \varepsilon\hat{r})/(2\varepsilon\hat{r})$. Equation (3) denotes resonant excitation from ∇P_h while the LHS of Eq. (2) shows the nonresonant one from plasma inertia. In the competition between resonant and nonresonant excitation, the latter wins, e.g., in the case of the low shear case, the LHS of Eq. (2) being dominant, can result in LLM. β_h in Eq. (3) is defined as the ratio of pressure of energetic ion to magnetic pressure. The variable ω_{ds} in Eq. (3) is the toroidal precessional frequency of energetic ions at the location of inertial layer. This frequency is proportional to beam energy E_b, and can be written as

$$\omega_{ds} = \frac{E_b}{mr_s\omega_0 R_0}, \quad (7)$$

where ω_0 is the cyclotron frequency. For the resonant mode, such as the FB instability, the real frequency of the mode,

being strongly dependent on ω_{ds}, is directly proportional to beam energy E_b. On the contrary, for the LLM, the real frequency of LLM hardly depends on beam energy due to the fact that the nonresonant excitation is dominant. The coefficients C_1, C_2, C_p and C_Ω in Eq. (2) are, respectively, given as follows:

$$C_1 = 2g_1 - \frac{2}{f_1} \int_0^1 \hat{r} d\hat{r} f(\hat{r}) g(\hat{r}),$$

$$C_2 = \frac{1}{2f_1} \int_0^1 d\hat{r} \hat{r}^2 g^2(\hat{r}) f'(\hat{r}),$$

$$C_p = f_1 + \frac{(1 - \hat{r}_0^2) f_1 - 1}{\hat{r}_0^2 (\sigma_\rho + 1)},$$

$$C_\Omega = f_1 g_1^2 - 2 \int_0^1 d\hat{r} \hat{r} f(\hat{r}) g^2(\hat{r}),$$

where $f_1 = f(1)$, $g_1 = g(1)$ and $A' = dA/d\hat{r}$ denotes the derivatives of f and g.

Equation (2) is the dispersion relation to study the FB mode and the LLM. By solving this nonlinear algebra equation of $\omega(= \omega_r + i\gamma)$, the features of the mode and the transition conditions between the FB mode and LLM can be obtained. In Sec. III, the numerical solutions of Eq. (2) are presented. However, in this section, in order to well understand the physical mechanism of LLM, it is valuable to give an analytical solution of Eq. (2) where the conditions $C_2 \ll C_1$ and for toroidal rotation $g_1 \ll 1$ are satisfied. Thus the terms of g_1 and C_2 in Eq. (2) can be neglected. Meanwhile the variables in the brackets of Eq. (3), $\hat{r} = 1$, K_c being independent of $\hat{r}$ are assumed. Besides, in the case of low shear, $K_c = K_2$ in Eq. (3), and for convenience, the analytical solutions of Eq. (2) are only given in the case of $\delta \hat{W}_c = 0$ and positive shear, i.e., $l = 0$ in Eq. (2). It is thus that Eqs. (2) and (3) are reduced to the following:

$$i \frac{\omega - \Omega_0}{\omega_A} \left[1 + i \frac{C_1 \Omega_0}{\hat{s}^2 \omega_A} \right] f_1 = \delta \hat{W}_k, \quad (7a)$$

$$\delta \hat{W}_k = - \left[\frac{\omega - \Omega_0}{\omega_{ds}} \ln \left(1 - \frac{K_2 \omega_{ds}}{\omega - \Omega_0} \right) \right] \frac{\beta_h R}{2 r_s I}$$

$$\times \int_{\sqrt{\alpha_1}}^{\sqrt{\alpha_2}} h(\alpha^2) d\alpha \int_{\hat{r}_1}^1 \hat{r} d\hat{r} \frac{dn_{0h}}{d\hat{r}} \frac{K}{q^2}. \quad (7b)$$

By substituting Eq. (7b) into Eq. (7a), the analytical solution can be obtained as follows:

$$\omega_r = \Omega_0 + \frac{K_c \omega_{ds}}{2} \left[\exp(-X) - \cos \frac{\eta}{\beta_h} \right] \left[\cosh(X) - \cos \frac{\eta}{\beta_h} \right]^{-1}, \quad (8)$$

$$\gamma = - \frac{K_c \omega_{ds}}{2} \left[\cosh(X) - \cos \frac{\eta}{\beta_h} \right]^{-1} \sin \frac{\eta}{\beta_h}, \quad (9)$$

where, $\eta = \frac{2 I \varepsilon \omega_{ds} f_1}{I' \omega_A}$, $X = \frac{\eta C_1 \Omega_0}{\hat{s}^2 \omega_A \beta_h}$, $I' = \int_{\sqrt{\alpha_1}}^{\sqrt{\alpha_2}} h(\alpha^2) d\alpha$ $\int_{\hat{r}_1}^1 \hat{r} d\hat{r} \frac{dn_{0h}}{d\hat{r}} \frac{K}{q^2}$. In Eqs. (8) and (9), the terms including Ω_0 are the nonresonant contributions from plasma rotation while other terms are resonant contributions from ∇P_h. The requirement of $X \gg 1$ indicates that the nonresonant excitation is dominant. Equation (9) shows that, without

rotation, the analytical growth rate can be reduced as $\gamma = -K_c \omega_{ds} [2 t g(0.5 \eta / \beta_h)]^{-1}$ and the critical β_h to drive the FB mode can be obtained by letting $\gamma = 0$, and $\beta_{h,\mathrm{crit}} = \eta/\pi$. Moreover, when β_h is sufficiently large, the growth rate $\gamma \propto \beta_h$, is a linear function of β_h, which can be checked in Sec. III A. But in the case of $X \gg 1$, a nonresonant mode can be driven by EIs and the critical β_h is

$$\beta_{h,\mathrm{crit}} = \frac{\eta C_1 \Omega_0}{\hat{s}^2 \omega_A X}. \quad (10)$$

Since $X \gg 1$, the critical β_h to drive the mode must be very low. Moreover, the real frequency of the mode is close to Ω_0 and the growth rate is low, which exhibits the LLM activity observed in experiments [5–10]. Here weak magnetic shear is one of the most important conditions to cause $X \gg 1$ to be satisfied. Besides, plasma rotation and the flat EI density profile (i.e., $I' \ll 1$) are another requirement to trigger LLM. But for the latter, according to Eq. (9), it is unfavorable for much too flattened EI density profile to drive LLM, and a sufficiently large gradient of EIs is necessary.

Equation (8) shows that, without rotation (i.e., $X = 0$), the mode has real frequency $\omega_r \propto \omega_{ds}$ and is typical of the FB mode. However, when $X \gg 1$, for instance, low shear, the mode is LLM. By letting the second term in Eq. (8) equal to τ, an infinitesimal quantity, an equation relating to critical Ω_0 causing the FB mode to transform into LLM can be obtained as follows:

$$\tau e^{2X} + (1 - 2\tau) \cos(\eta/\beta_h) e^X - (1 - \tau) = 0. \quad (11)$$

In general, $\beta_h \sim O(\eta)$ and $\cos(\beta_h/\eta) \sim 0.5$. By solving Eq. (11) and taking the limit as τ approaches zero of X, this gives the dependence of Ω_0 on $\hat{s}$ as follows:

$$\frac{\Omega_0}{\hat{s}^2} = \frac{\omega_A \ln 2}{|C_1|}. \quad (12)$$

Equation (12) is the critical Ω_0 causing the FB mode to transform into or from LLM in low shear plasmas.

III. THE NUMERICAL RESULTS

In this section, the numerical solutions of Eq. (2) are presented under the conditions of positive magnetic shear and the negative one, respectively. Since the LLM was observed in both monotonic and nonmonotonic q profile plasmas [6,7,12–14], it is necessary to discuss the transition between the FB mode and LLM for different safety factor profiles, for instance, in plasmas with positive (i.e., monotonic q profile) and negative (i.e., nonmonotonic q profile) magnetic shear. In Sec. III A, the features of the LLM and the FB mode for the former are discussed while those for the latter are given in Sec. III B.

HL-2A is a medium size tokamak with minor radius $a = 40$ cm and major radius $R_0 = 165$ cm, the toroidal magnetic field is $B_0 = 1.3$ T, the on-axis electron density is $n_e = 2.5 \times 10^{19}$ m^{-3} during near-axis NBI heating, the temperature of thermal particles $T_i = T_e = 1.5$ keV [22]. The beam energy $E_b = 40$ keV. The on-axis Alfven frequency is $\omega_A = 3.4 \times 10^6$ rad/s. Figure 2(a) shows safety factor profiles inside $q = 1$ (or $q_{\min}$) surface with the $q = 1$ (or $q_{\min}$) flux surface being at $r_s = a/2$ [12], and Fig. 2(b) is EI density profiles (blue

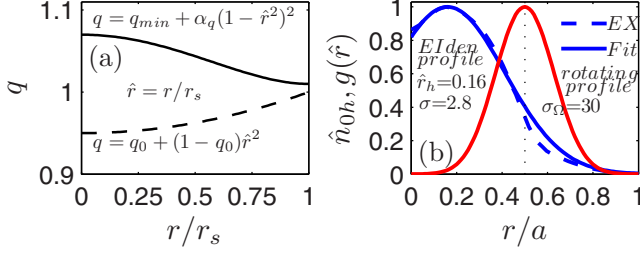FIG. 2. (a) Safety factor profile inside $q = 1$ ($q_{\min}$) surface, the dashed (solid) line denotes positive (negative) magnetic shear. (b) The profiles of EI density (blue lines) and rotation (red line). The dashed line is experimental EI density profile given by ONETWO and the solid blue one is plotted by $n_{0h}(r) \sim \exp[-\sigma^2(r - r_h)^2]$ with $\sigma = 2.8$, $\hat{r}_h = 0.16$. The dotted line denotes the position of $q = 1$ ($q_{\min}$) flux surface.

lines) and plasma rotation profile (red line). The on-axis safety factor is set as $q_0 = 0.96$ for positive magnetic shear and $q_{\min} = 1.03$, $\alpha_q = 0.06$ for negative one. The weak and strong magnetic shear can be realized by adjusting q_0 and α_q. In Fig. 2(a), the dashed and solid lines are plotted by using Eqs. (5) and (6), respectively. In Fig. 2(b), the dashed blue line is the experimental EI density profile calculated with ONETWO code and the solid blue one is plotted by $n_{0h}(r)$. The solid red line is the plasma rotation profile plotted by $g(r)$ with $\hat{r}_\Omega = 0.5$, $\sigma_\Omega = 30$. In the case of toroidal rotation, it is necessary to set $\hat{r}_\Omega = 0$.

A. The long-lived mode in weak magnetic shear plasmas with monotonic q profile

In this section, we first discuss the transition between the FB mode and LLM with the monotonic q profile (i.e., the positive magnetic shear) by solving Eq. (2). According to Eq. (5), the magnetic shear at the position of $q = 1$ flux surface is defined by $\hat{s} = r_s q_s'$. Figure 3 is real frequency (a) and growth rate (b) of LLM (red lines) and the FB mode (blue lines) as functions of β_h for different beam energy with $\Omega_0 = 2 \times 10^4$ rad/s, $\hat{r}_\Omega = 0$, $\sigma_\Omega = 7$ and $\sigma_\rho = 2$. The mag-
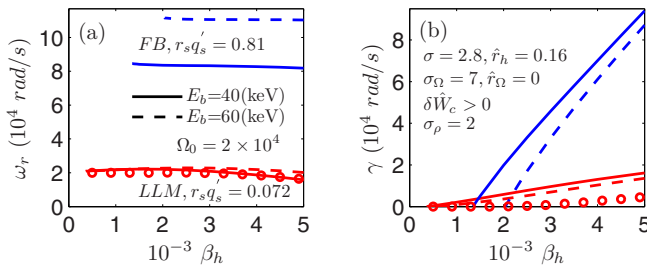

FIG. 3. Real frequencies (a) and growth rates (b) of LLM (red lines) and the FB mode (blue ones) as functions of β_h for different beam energy (E_b) with $\Omega_0 = 2 \times 10^4$ rad/s, $\hat{r}_\Omega = 0$, $\sigma_\Omega = 7$, $\sigma_\rho = 2$, $\sigma = 2.8$ and $\hat{r}_h = 0.16$. The magnetic shear $\hat{s} = 0.072$ for LLM and $\hat{s} = 0.81$ for FB. The circles are theory results while other lines are the numerical results by solving Eq. (2). The solid red and blue lines denote beam energy $E_b = 40$ keV whereas the dashed red and blue ones represent $E_b = 60$ keV.

netic shear $\hat{s} = 0.072$ for LLM and $\hat{s} = 0.81$ for the FB mode. The solid lines denote the case of $E_b = 40$ keV whereas the dashed lines represent that of $E_b = 60$ keV. The circles are theoretical calculations by using Eqs. (8) and (9) while other lines are numerical results given by solving Eq. (2). The blue lines show that the FB mode can be excited by EIs when β_h exceeds a threshold. The real frequency of FB is proportional to beam energy E_b and the growth rate increases with β_h. The red lines show an interesting result. In the case of weak magnetic shear, the mode, similar to the FB mode, can be driven by energetic ions when β_h exceeds a threshold. The growth rate of the mode increases with β_h. Especially, it is interesting that the real frequency of the mode, almost independent of beam energy, is equal to Ω_0, the on-axis toroidal rotation frequency, which is highly similar to the features of LLM observed in experiments [5–10]. This result implies that LLM is a nonresonant mode driven by EIs due to zero frequency in static plasmas. Although the resonant excitation from ∇P_h of EIs for LLM is not dominant any more, the critical β_h to drive LLM shows that, without EIs, the mode is stable and difficult to be observed in experiment. By comparing with the FB mode, LLM is easier to be excited by EIs than the FB mode due to sufficiently low critical β_h. The solid red lines and circles in Fig. 3(b) show that the growth rates of LLM given by theory are different from those of numerical calculations. The differences mainly result from the neglected terms in Eq. (2). By comparing the red lines with blue ones in Fig. 3, it can be learnt that LLM instability only occur under the condition of weak magnetic shear and the mode is characterized by zero real frequency in static plasmas. On the contrary, in the case of strong magnetic shear, the mode behaves as the FB instabilities with mode frequency being related to the toroidal precessional frequency of EIs. Thus different magnetic shear is used to discuss the problems in this section.

An analytical solution predicts a critical rotation frequency to cause the FB mode to evolve into LLM in low shear plasmas. Moreover, the mode frequency of LLM is strongly dependent on rotation frequency. Consequently, it is worthwhile discussing the influence of toroidal rotation on the mode in weak magnetic shear plasmas, so as to understand the physical mechanism cuasing the transition between the FB mode and LLM. The lines in Fig. 4 are real frequency (a) and growth rate (b) of the mode as functions of Ω_0 for different beam energy with $\hat{s} = 0.072$, $\hat{r}_\Omega = 0$, $\sigma_\Omega = 7$. The solid and dashed lines represent beam energy $E_b = 40$ and 60 (keV), respectively. The dotted lines are theory calculations using Eqs. (8) and (9). It can be seen from Fig. 4(a) that, in rotating and weak magnetic shear plasmas, the real frequency of the mode first decreases with Ω_0, when toroidal rotation frequency exceeds a threshold (say 8 krad/s), and linearly increases with Ω_0. When $\Omega_0 > 8$ krad/s, the real frequency of the mode is equal to the on-axis toroidal rotation frequency, moreover independent of beam energy, which is in good agreement with the LLM observed in experiments [5–10]. Also, the measured frequency of LLM at the location of minor radius $r = 0.2$ cm in HL-2A is around 10.5 kHz (i.e., 66 krad/s, given by the dashed pink line in Fig. 3(c) in Ref. [9]) which agrees well with that in Fig. 4(a). On the other hand, Fig. 4(a) also shows that, in static plasmas, e.g., $\Omega_0 = 0$, the mode is typical of the FB mode due to the real frequency of the mode being proportional to beam
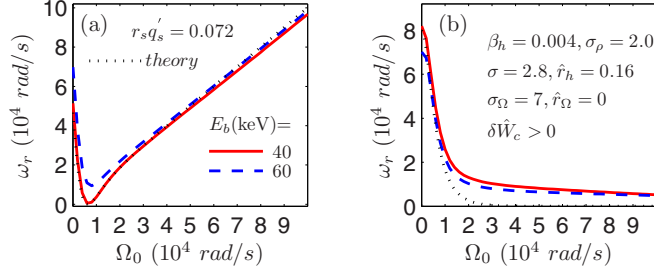
FIG. 4. Real frequencies (a) and growth rates (b) of the mode as functions of toroidal rotation frequency with $\hat{s} = 0.072$, $\hat{r}_\Omega = 0$, $\sigma_\Omega = 7$, $\sigma_\rho = 2$, $\beta_h = 0.004$, $E_b = 40\,\mathrm{keV}$ for solid lines and $E_b = 60\,\mathrm{keV}$ for dashed lines. The dotted lines denote theory calculation with the same parameters as the red lines while other lines are the numerical results by solving Eq. (2). The solid red and dotted lines denote beam energy $E_b = 40\,\mathrm{keV}$ whereas the dashed blue ones represent $E_b = 60\,\mathrm{keV}$.

FIG. 6. Real frequencies (a) and growth rates (b) of LLM (red lines) and the FB mode (blue ones) as functions of β_h for different beam energy with $\Omega_0 = 2 \times 10^4\,\mathrm{rad/s}$, $\hat{r}_\Omega = 0$, $\sigma_\Omega = 7$, $\sigma_\rho = 2$ and $q_{\min} = 1.03$. The magnetic shear $\hat{s} = 0.056$ for LLM and $\hat{s} = 1.28$ for the FB mode. The solid red and blue lines denote beam energy $E_b = 40\,\mathrm{keV}$ whereas the dashed red and blue ones represent $E_b = 80\,\mathrm{keV}$.

energy. Since LLM rotates with plasma, it must appear static in the plasma frame, implying that LLM fails to resonate with energetic ions. Consequently, it is difficult for LLM to cause significant EIs loss, which agrees well with the experiments [15,16]. Figure 4(b) shows that the growth rate of the mode monotonically decreases with Ω_0 and the growth rate of LLM is much less than that of the FB mode. Figure 4 also indicates that the transition between the FB mode and LLM only occurs in rotating and weak magnetic shear plasmas. The minimum ω_r value in Fig. 4(a) shows that the critical Ω_0 to trigger transition is around 8 krad/s, which is almost independent of beam energy and agrees with Eq. (12). In the case of strong magnetic shear, for instance, $\hat{s} = 0.81$ (not plotted in Fig. 4), the real frequency of the mode, being proportional to E_b, monotonically increases with Ω_0, indicating that the FB mode is difficult to evolve into LLM whatever the speed of plasma rotation is. Similar discussions will be done in the case of nonmonotonic q profile in Sec. III B, for example, the results in Fig. 7.

Besides rotation, magnetic shear is another important condition to cause transitions between the FB mode and LLM. The influences of magnetic shear in the case of the monotonic safety factor profile on the modes are given in Fig. 5, where the dashed, dash-dotted, and solid lines denotes beam energy $E_b = 40, 60$ and 80 (keV), respectively. The lines in Fig. 5(a)

show that, in the low shear region, for instance $\hat{s} < 0.1$, real frequencies of the modes are almost equal to the toroidal rotation frequency of bulk plasmas. On the contrary, in the high shear region, e.g., $\hat{s} > 0.1$, real frequency of the mode increase with magnetic shear and are proportional to beam energy E_b. The mode, in low shear plasmas, exhibits features of LLM while in strong shear plasmas, shows that of the FB mode. It can be concluded that weak shear is the necessary condition to trigger LLM, which agrees with experiments and theory.

B. The long-lived mode in weak magnetic shear plasmas with nonmonotonic q profile

Besides the LLM observed in positive magnetic shear plasmas, in MAST weakly reversed shear plasmas, LLM was also observed under the condition of nonmonotonic q profile with a minimum at r_s (the minimum q value position) where $q'(r_s) = 0$ and $q(r_s)$ is slightly above one [6–8]. By using the q profile of Eq. (6) or the solid line in Fig. 2(a), the LLM in reversed shear plasmas can be studied by numerically solving Eq. (2). However, considering $dq/dr = 0$ at the location of $q = q_{\min}$ (i.e., the inertial layer), the safety factor profile must be expanded to the second order at the position of $q = q_{\min}$ flux surface (see the Appendix). Moreover, the value of d^2q/dr^2 is proportional to that of dq/dr inside $q = q_{\min}$ magnetic flux surface. Therefore the local magnetic shear can be defined by $\hat{s} = r_s^2 q_s''$. The strong and weak magnetic shear can, respectively, be realized by changing the values of α_q in Eq. (6).

The results shown in Fig. 6 are, in reversed shear plasmas, the real frequencies (a) and growth rates (b) of LLM (red lines) and the FB mode (blue ones) as functions of β_h for different beam energy with $q_{\min} = 1.03$, $\Omega_0 = 2 \times 10^4\,\mathrm{rad/s}$, $\hat{r}_\Omega = 0$, $\sigma_\Omega = 7$. The local magnetic shear $\hat{s} = 0.056$ for LLM and $\hat{s} = 1.28$ for the FB mode. The solid and dashed lines represent beam energy $E_b = 40$ and 80 (keV), respectively. The red lines in Fig. 6(a) show that, LLM in weakly reversed shear plasmas, similar to that in positive ones, is characterized by frequency close to on-axis toroidal rotation frequency. Moreover the real frequency of LLM, almost independent of E_b, stays unchanged with increasing β_h and is roughly equal to
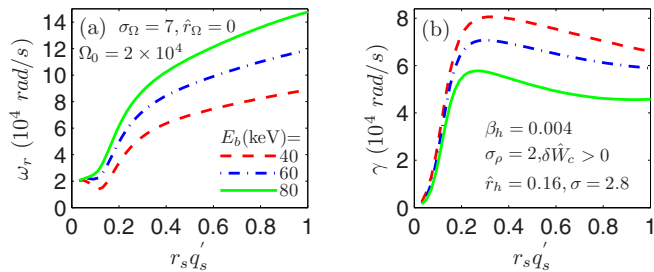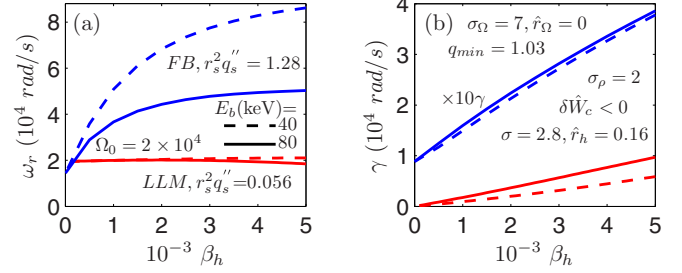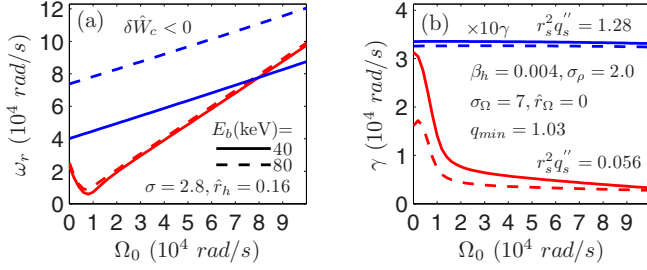

FIG. 5. Real frequencies (a) and growth rates (b) of the mode as functions of local magnetic shear with $\sigma_\Omega = 7$, $\hat{r}_\Omega = 0$, $\beta_h = 0.004$, $\sigma_\rho = 2$, $\Omega_0 = 2 \times 10^4\,\mathrm{rad/s}$. The dashed, dash-dotted, and solid lines denote the cases of $E_b = 40, 60$ and 80 (keV), respectively.

FIG. 7. Real frequencies (a) and growth rates (b) of the modes as functions of Ω_0 with $\hat{r}_\Omega = 0$, $\sigma_\Omega = 7$, q_{min} $q_{min} = 1.03$, $\beta_h = 0.004$, the red and blue lines represent $\hat{s} = 0.056$ and $\hat{s} = 1.28$, respectively. The solid red and solid blue lines denote beam energy $E_b = 40$ keV whereas the dashed red and dashed blue ones represent $E_b = 80$ keV.

FIG. 8. Real frequencies (a) and growth rates (b) of the mode as functions of local magnetic shear with $\sigma_\Omega = 7$, $\hat{r}_\Omega = 0$, $\beta_h = 0.004$, $q_{min} = 1.03$, $\sigma_\rho = 2$, $\Omega_0 = 2 \times 10^4$ rad/s. The solid and dashed lines denote beam energy $E_b = 40$ and 80 (keV), respectively.

to 2×10^4 rad/s. The blue lines in Fig. 6(a) indicate that, in strong magnetic shear plasmas, when β_h is big enough, the real frequency of the mode is proportional to E_b and the mode behaves as the FB-like instability. The red lines in Fig. 6(b) show that LLM can only be excited by EIs when β_h exceeds a threshold. Similar to those in Fig. 3, the motivation of different magnetic shear being employed to discuss the problem is that, in the case of nonmonotonic q profile, LLM bursts can only occur under the condition of weakly reversed magnetic shear.

Shown in Fig. 7 is real frequency and growth rate of the modes as functions of Ω_0 in reversed magnetic shear plasmas. The red lines represent LLM with $\hat{s} = 0.056$ (i.e., weak magnetic shear) while the blue lines do the FB mode with $\hat{s} = 1.28$ (i.e., strong magnetic shear). Figure 7(a) shows that, in weakly reversed shear plasmas, similar to the counterparts in Fig. 4, LLM occurs when rotation frequency exceeds a threshold (e.g., 8 krad/s); moreover the mode frequency of LLM, being almost independent of beam energy, is equal to Ω_0, which is similar to the experimental observations in MAST [5–7]. But in strong shear plasmas (blue lines), the real frequency of the mode, being proportional to E_b, linearly increases with Ω_0, and the mode exhibits the FB activities. It can be seen from the blue lines that the real frequency of the FB mode is related to the characteristic frequency of EIs, and the transition between the FB mode and LLM is difficult in strong magnetic shear plasmas. Therefore, the different magnetic shear is used to discuss the possibility of transition between the FB mode and LLM. Figure 7(b) also shows that the growth rate of LLM is much less than that of the FB.

Especially, the red lines in Fig. 7(a) show that, in the case of nonmonotonic q profile, the real frequency of the mode even at $\Omega_0 = 0$, much different from the counterparts in Fig. 4(a), hardly depends on E_b, which indicates that in weakly reversed shear plasmas, the FB mode (or internal kink mode) can be nonresonantly excited by energetic ions and the nonresonant excitation source mainly comes from the inertial term, for example, the first term in the square brackets of Eq. (2).

Figure 8 gives the dependence of real frequency (a) and growth rate (b) of the mode on magnetic shear $\hat{s}$ with $q_{min} = 1.03$, $\Omega_0 = 2 \times 10^4$ rad/s. The results are similar to those shown in Fig. 5. For low shear regions, e.g., $\hat{s} < 0.1$, the real frequency of the mode is approximately equal to toroidal rotation frequency on the magnetic axis, and the mode exhibits
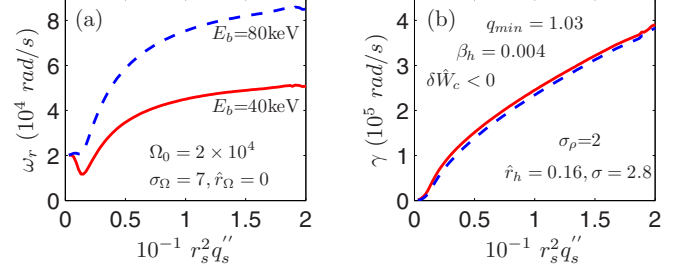
the features of the LLM. On the contrary, when the magnetic shear is sufficiently large, the real frequency of the mode is proportional to beam energy E_b, and the mode behaves as FB-like instabilities. Consequently, in rotating plasmas with a nonmonotonic safety factor profile, the FB mode can also evolve into the LLM only if the magnetic shear inside $q = q_{min}$ flux surface is sufficiently weak.

IV. CONCLUSIONS

LLMs driven by energetic ions in rotating plasmas are studied by using a new dispersion relation. It is found that, in low shear and rotating plasmas, LLM can be nonresonantly induced by energetic ions when β_h is bigger than a critical value, and the real frequency of LLM, independent of the energy of NBI ions, is proportional to the toroidal rotation frequency of bulk plasma on magnetic axis. The key conditions to induce LLM are weak magnetic shear and plasma rotation; moreover LLM activity cannot occur without EIs. The FB mode, only in weak magnetic shear plasmas, usually transforms into LLM when plasma rotation frequency is bigger than a critical value. The modified inertial term from plasma rotation plays a crucial role in causing the FB mode to transform into LLM which is a branch of nonresonant MHD mode.

ACKNOWLEDGMENTS

APPENDIX: THE DISPERSION RELATION IN TOROIDAL ROTATING PLASMAS

The perturbed displacement of plasma is taken as $\vec{\xi} = (\xi_r \vec{e}_r + \xi_\theta \vec{e}_\theta)e^{-i\omega_1 t}$. Thus, the relation between perturbed velocity and displacement of plasma is $\delta\vec{v} = -i\omega_1\vec{\xi}$ with $\omega_1 = \omega - \Omega_0$. By substituting the perturbed velocity into Eq. (1), an inner product of Eq. (1) with $\vec{\xi}^*$ is taken and integrates over plasma volume inside the $q = 1$ surface. Eq. (1) can be

rewritten as follows:

$$-\int d^3x\rho\omega_1^2\vec{\xi}\bullet\vec{\xi}^* - \int d^3x\rho\vec{a}_c\bullet\vec{\xi}^* = \int d^3x(\delta\vec{J}\times\vec{B} + \vec{J}\times\delta\vec{B} - \nabla\delta p_c)\bullet\vec{\xi}^* - \int d^3x(\nabla\bullet\delta\vec{\vec{p}}_h)\bullet\vec{\xi}^*, \quad (A1)$$

where $\vec{a}_c = -2i\omega_1\vec{\xi}\times\vec{\Omega} + \nabla\rho\bullet\vec{\xi}\vec{V}_0 + \nabla V_0/\rho + i\omega_1\vec{\xi}\bullet\nabla V_0 + i\omega_1\vec{V}_0\bullet\nabla\vec{\xi}$ with $\vec{V}_0 = \vec{\Omega}\times\vec{R}$. The perturbed pressure of bulk plasmas is $\delta p_c = -\xi\cdot\nabla P_{eq} - \Gamma P_{eq}\nabla\cdot\xi$ with P_{eq} being the equilibrium pressure. The perturbed current density is $\delta\vec{J} = \nabla\times\delta\vec{B}/\mu_0$, the perturbed magnetic field is $\delta\vec{B} = \nabla\times(\vec{\xi}\times\vec{B})$, the pressure of energetic ions is $\delta p_{h//} = \int\delta f_h mv_{//}^2 d^3v$, $\delta p_{h\perp} = \int\delta f_h\mu B d^3v$. The distribution function of energetic ions δf_h is given in Ref. [20]. Meanwhile, it is easy to find that the effective inertial force acceleration a_c in Eq. (1) is self-adjoint. By substituting these perturbed variables into Eq. (A1), the following dispersion relation in toroidal geometry can be obtained:

$$\delta I + \delta W_{MHD} + \delta W_k = 0, \quad (A2)$$

where, the kinetic energy due to plasma inertia δI, the perturbed potential energy δW_{MHD} from bulk plasma, and the perturbed potential energy δW_k from energetic ions are given as follows:

$$\delta I = -\frac{1}{2}\int\rho d^3x[\omega_1^2|\vec{\xi}|^2 + \vec{a}_c\bullet\vec{\xi}^*], \quad (A3)$$

$$\delta W_{MHD} = \frac{1}{2}\int d^3x(\nabla\delta p_c - \delta\vec{J}\times\vec{B} - \vec{J}\times\delta\vec{B})\bullet\vec{\xi}^* = \frac{1}{2}\int d^3x[|\delta\vec{B}|^2 - \vec{J}_{//}(\vec{\xi}_\perp\times\vec{b})\bullet\delta\vec{B}_\perp - 2(\vec{\xi}_\perp\bullet\nabla p_{eq})(\vec{\xi}_\perp\bullet\vec{\kappa})$$

$$+ B^2(\nabla\bullet\vec{\xi}_\perp + 2\vec{\xi}_\perp\bullet\vec{\kappa})^2 + \Gamma p_{eq}(\nabla\bullet\vec{\xi})^2], \quad (A4)$$

$$\delta W_k = \frac{1}{2}\int d^3x(\nabla\bullet\delta\vec{\vec{p}}_h)\bullet\vec{\xi}^* = 2^{9/2}\pi^3 m_h\int R_0 r dr\int d\frac{\mu B}{E}\int_0^\infty dE E^{5/2}K_b\frac{\bar{J}_0^* Q\bar{J}_0}{\omega_d - \omega_1}, \quad (A5)$$

where, $K_b = \frac{1}{2\pi}\oint\frac{d\theta}{\sqrt{1-\mu B/E}}$, $Q = \omega_1\frac{\partial F_{0h}}{\partial E} - \frac{1}{\omega_0 r}\frac{\partial F_{0h}}{\partial r}$, $J_0 = \frac{\mu B}{2E}\nabla\bullet\vec{\xi}_\perp - (1-\frac{3\mu B}{2E})\vec{\xi}_\perp\bullet\vec{\kappa}$ with $\vec{\kappa} = \vec{b}\bullet\nabla\vec{b} = -\vec{e}_R/R_0$ being the curvature of the magnetic field line and the vector along the major radius is $\vec{e}_R = \vec{e}_r\cos\theta - \vec{e}_\theta\sin\theta$. $\bar{J}_0 = \oint\frac{J_0 dl}{v_{//}}/\oint\frac{dl}{v_{//}}$, the parallel velocity of energetic ions is $v_{//}\sim\sqrt{1-\mu B/E} = \sqrt{2\alpha\varepsilon\hat{r}}\sqrt{k^2 - \sin^2\theta/2}$ with argument $k^2 = (1/\alpha - 1 + \varepsilon\hat{r}))/(2\varepsilon\hat{r})$. For trapped particles, the turning point θ_b, determined by letting $v_{//} = 0$, is $\sin(\theta_b/2) = k$. When the relation $\nabla\bullet\vec{\xi}_\perp = -2\vec{\xi}_\perp\bullet\vec{\kappa}$ is used, the variable J_0 can be reduced to $J_0 = (\frac{\mu B}{2E} - 1)\vec{\xi}_\perp\bullet\vec{\kappa}$. The steplike trial function inside $q = 1$ (q_{min}) can be written as $\vec{\xi}_\perp = \xi_0(\vec{e}_r + i\vec{e}_\theta)$. The averaged toroidal precessional frequency of energetic ions is $\omega_d = \omega_{ds}qK_c\hat{E}/\hat{r}$ with $\hat{E} = E/E_b$ and E is energy of energetic ions. The equilibrium distribution function of energetic ions is $F_{0h}(r, \alpha, E) = n_{0h}(r)h(\alpha)E^{-3/2}$. In Eq. (A5), the variables K_b and the averaged J_0 can be reduced in the following manner, respectively:

$$K_b = \frac{1}{\pi}\int_0^{\theta_b}\frac{d\theta}{\sqrt{1-\alpha+\alpha\varepsilon\cos\theta}} = \frac{1}{\pi\sqrt{2\alpha\varepsilon\hat{r}}}\int_0^{\theta_b}\frac{d\theta}{\sqrt{k^2-\sin^2(\theta/2)}}\underset{\text{let}\quad\sin(\theta/2)=k\cos\phi}{=}\frac{1}{\pi\sqrt{2\alpha\varepsilon\hat{r}}}\int_{\pi/2}^0\frac{-2k\sin\phi}{k\sin\phi}\frac{d\phi}{\cos(\theta/2)}$$

$$= \frac{1}{\pi}\sqrt{\frac{2}{\alpha\varepsilon\hat{r}}}\int_0^{\pi/2}\frac{d\phi}{\sqrt{1-k^2\sin^2\phi}} = \frac{1}{\pi}\sqrt{\frac{2}{\alpha\varepsilon\hat{r}}}K(k^2),$$

$$\bar{J}_0 = \oint\frac{J_0 dl}{v_{//}}\Big/\oint\frac{dl}{v_{//}} = \int_0^{\theta_b}\frac{(\mu B/2E-1)\vec{\xi}_\perp\bullet\vec{\kappa}d\theta}{\sqrt{1-\mu B/E}}\Big/\int_0^{\theta_b}\frac{d\theta}{\sqrt{1-\mu B/E}} = \frac{1}{\pi K_b}\int_0^{\theta_b}\frac{(\mu B/2E-1)\vec{\xi}_\perp\bullet\vec{\kappa}d\theta}{\sqrt{1-\mu B/E}}$$

$$= \frac{-1}{2\pi K_b}\int_0^{\theta_b}\left[\sqrt{1-\mu B/E} + \frac{1}{\sqrt{1-\mu B/E}}\right]\vec{\xi}_\perp\bullet\vec{\kappa}d\theta \approx \frac{-1}{2\pi K_b}\int_0^{\theta_b}\frac{\vec{\xi}_\perp\bullet\vec{\kappa}d\theta}{\sqrt{1-\mu B/E}} = \frac{\xi_0}{2\pi R_0 K_b}\int_0^{\theta_b}\frac{\cos\theta d\theta}{\sqrt{1-\mu B/E}}$$

$$= \frac{\xi_0}{2\pi R_0 K_b\sqrt{2\alpha\varepsilon\hat{r}}}\int_0^{\theta_b}\frac{\cos\theta d\theta}{\sqrt{k^2-\sin^2\theta/2}} = \frac{\xi_0}{2\pi R_0 K_b\sqrt{2\alpha\varepsilon\hat{r}}}\int_{\pi/2}^0\frac{1-2\sin^2(\theta/2)}{k\sin\phi}\cdot\frac{-2k\sin\phi}{\cos(\theta/2)}d\phi$$

$$= \frac{\xi_0}{2R_0 K(k^2)}\int_{\pi/2}^0\frac{2k^2\cos^2\phi - 1}{\sqrt{1-k^2\cos^2\phi}}d\phi = \frac{\xi_0}{2R_0}\frac{2E-K}{K},$$

where K and E are the first and second complete elliptical integrals, respectively. It should be mentioned that in the above equations, the poloidal angle θ denotes the usual geometrical variable. By substituting these variables, for instance, K_b, $\bar{J}_0$ and ω_d, into Eq. (A5) and neglecting the terms being directly proportional to $\varepsilon(= r_s/R_0)$, the kinetic contribution from energetic ions, i.e., Eq. (3) in Sec. II can be obtained after integrating over energy from zero to infinity. The MHD contribution from bulk plasmas, i.e., Eq. (A4) is given in Ref. [21] in detail.

When the toroidal rotation is taken into account, the plasma density is a function of minor radius r and poloidal angle θ, i.e., $\rho = \rho(r,\theta)$ which can be written as follows:

$$\rho(r,\theta) = \rho(r) + \frac{\rho(r) m_i \Omega^2(r) R_0^2}{2kT(r)} \cdot \frac{r}{R_0} \cos\theta, \tag{A6}$$

where $T(r) = T_0 u(r)$ is plasma temperature profile and k is Boltzman constant. The modified inertial term Eq. (A3) can be reduced in the following manner:

$$
\begin{aligned}
\delta I &= -\frac{1}{2}\int \rho d^3x \left[\omega_1^2|\vec{\xi}|^2 - 2i\omega_1\vec{\xi} \times \vec{\Omega} + \nabla\rho \bullet \vec{\xi}\vec{V}_0 \bullet \nabla\vec{V}_0/\rho + i\omega_1\vec{\xi}\bullet\nabla\vec{V}_0 + i\omega_1\vec{V}_0\bullet\nabla\vec{\xi}\right]\bullet\vec{\xi}^* \\
&= -\frac{\omega_1}{2}\int \rho d^3x \left[\omega_1|\vec{\xi}|^2 - \left(\frac{\xi_r d\rho}{\omega_1\rho dr} + \frac{\xi_\theta d\rho}{\omega_1\rho r d\theta}\right)\frac{V_0^2}{R}\vec{e}_R + i\left(\xi_r\frac{dV_0}{dr}\vec{e}_\varphi + \xi_\theta\frac{dV_0}{rd\theta}\vec{e}_\varphi\right) + \frac{V_0}{R}\vec{\xi}\right]\bullet\vec{\xi}^* \\
&= -\frac{\omega_1}{2}\int \rho d^3x \left[\omega_1|\vec{\xi}|^2 - \left(\frac{\xi_r d\rho}{\omega_1\rho dr} + \frac{\xi_\theta d\rho}{\omega_1\rho r d\theta}\right)\Omega^2 R_0\left(1 + \frac{r}{R_0}\cos\theta\right)\vec{e}_R\bullet\vec{\xi}^* + \Omega|\vec{\xi}|^2\right],
\end{aligned}\tag{A7}
$$

note, in Eq. (A7), $\rho = \rho(r,\theta)$, and the term $\vec{\xi}\times\vec{\Omega}$ is neglected due to $(\vec{\xi}\times\vec{\Omega})\bullet\vec{\xi}^* = 0$ for toroidal rotation. Considering the condition $\nabla\bullet\vec{\xi} = 0$, i.e., the displacement is incompressible, the poloidal perturbed displacement can be taken as $\xi_\theta = id(r\xi_r)/dr$. By substituting Eq. (A6) into Eq. (A7), which can be further reduced in the following manner:

$$
\begin{aligned}
\delta I &= -\frac{\omega_1}{2}\int_0^{r_s}dr\int_0^{2\pi}rd\theta\left[\rho(r,\theta)\omega_1\left(\xi_r^2 + \left|\frac{dr\xi_r}{dr}\right|^2\right) - \left(\frac{\xi_r d(r,\theta)}{\omega_1 dr} + \frac{\xi_\theta d(r,\theta)}{\omega_1 r d\theta}\right)\Omega^2 R_0\right.\\
&\quad\left.\times\left(\xi_r^*\cos\theta - \xi_\theta^*\sin\theta + \frac{r}{R_0}(\xi_r^*\cos^2\theta - \xi_\theta^*\cos\theta\sin\theta)\right) + \rho(r,\theta)\Omega\left(\xi_r^2 + \left|\frac{dr\xi_r}{dr}\right|^2\right)\right]\\
&= -\frac{\omega_1}{2}\int_0^{r_s}dr\int_0^{2\pi}rd\theta\left[\left(\rho(r) + \frac{\rho(r)m_i\Omega^2(r)R_0}{2kT(r)}r\cos\theta\right)\omega_1\left(\frac{rd\xi_r}{dr}\right)^2\right.\\
&\quad- \Omega^2 R_0\left(\frac{\xi_r}{\omega_1}\left(\frac{d\rho(r)}{dr} + \frac{d}{dr}\frac{r\rho(r)m_i\Omega^2(r)R_0}{2kT(r)}\cos\theta\right) - \frac{\xi_\theta}{\omega_1}\frac{\rho(r)m_i\Omega^2(r)R_0}{2kT(r)}\sin\theta\right)(\xi_r^*\cos\theta - \xi_\theta^*\sin\theta\\
&\quad\left.+ r(\xi_r^*\cos^2\theta - \xi_\theta^*\cos\theta\sin\theta)/R_0) + \left(\rho(r) + \frac{\rho(r)m_i\Omega^2(r)R_0^2}{2kT(r)}\cdot\frac{r}{R_0}\cos\theta\right)\Omega\left(\xi_r^2 + \left|\frac{dr\xi_r}{dr}\right|^2\right)\right]\\
&= -\frac{\pi\omega_1}{2}\int_0^{r_s}rdr\left[2\rho(r)\omega_1\left(\frac{rd\xi_r}{dr}\right)^2 - \frac{\xi_r^2\Omega^2}{\omega_1}\left(\left(r\frac{d\rho(r)}{dr} + \frac{d}{dr}\frac{r\rho(r)m_i\Omega^2(r)R_0^2}{2kT(r)}\right)\right.\right.\\
&\quad\left.+\left(\xi_r^2 + \left|\frac{dr\xi_r}{dr}\right|^2\right)\frac{\rho(r)m_i\Omega^2(r)R_0^2}{2kT(r)\xi_r^2}\right) + 2\rho(r)\Omega\left(\xi_r^2 + \left|\frac{dr\xi_r}{dr}\right|^2\right)\right]\\
&= -\frac{\pi\rho_0\omega_1}{2}\int_0^{r_s}rdr\left[2f(r)\left(\omega_1 + \Omega_0 g(r) - \frac{\Omega_0^2}{\omega_1}\frac{m_i\Omega_0^2 R_0^2}{4kT_0}\frac{g^4(r)}{u(r)}\right)\left(\frac{rd\xi_r}{dr}\right)^2 + 2f(r)\left[2\Omega_0 g(r)\right.\right.\\
&\quad- \frac{\Omega_0^2}{\omega_1}\frac{m_i\Omega_0^2 R_0^2}{2kT_0}\frac{g^4(r)}{u(r)}\right]r\xi_r\frac{d\xi_r}{dr} + \xi_r^2\left(4\Omega_0 f(r)g(r) - \frac{\Omega_0^2}{\omega_1}rg^2(r)\frac{df(r)}{dr}\right.\\
&\quad\left.\left.- \frac{\Omega_0^2}{\omega_1}\frac{m_i\Omega_0^2 R_0^2}{2kT_0}g^2(r)\frac{d}{dr}\frac{f(r)g^2(r)r}{u(r)} - \frac{2\Omega_0^2}{\omega_1}\frac{m_i\Omega_0^2 R_0^2}{2kT_0}\frac{f(r)g^4(r)}{u(r)}\right)\right].
\end{aligned}\tag{A8}
$$

The perturbed plasma displacement in the radial direction ξ_r in Eq. (A8) satisfies Euler equation,

$$\frac{d}{dx}\left[[3\omega_1^2 - \omega_A^2(q-1)^2]\frac{d\xi_r}{dx}\right] = 0, \tag{A9}$$

with $x = (r - r_s)/r_s$. Within the inertial layer, i.e., at the location of $r = r_s$, the safety factor profile $q(r)$ should be expanded to the second order in x as

$$q(r) = q(r_s) + r_s q'(r_s)x + \frac{r_s^2 q''(r_s)}{2}x^2. \tag{A10}$$

For monotonic q profile, By retaining the first two terms in Eq. (A10) (i.e., $q = 1 + r_s q'(r_s)x$) and substituting them into Eq. (A9), the solution of Eq. (A9) is then a hyperbolic tangent function which can be written as

$$\xi_r = \frac{\xi_0}{2}\left[1 - \frac{2}{\pi}artg\left(\frac{x}{\Delta}\right)\right], \tag{A11}$$

with $\Delta = \sqrt{3}R_0\omega_1/(iq'_s V_A)$. When the width of inertial layer (or Δ) is sufficiently small, Eq. (11) can be expanded to a linear function of x (or $r - r_s$) in the vicinity of $q = 1$ flux surface, i.e., the perturbed displacement of plasma in the inertial layer can be replaced by $\xi_r = 0.5\xi_0[1 - 2(r - r_s)/(\pi\Delta)]$. Considering the plasma displacement ξ_r being constant inside $q = 1$ surface, thus the following steplike function of ξ_r can be used to calculate the perturbed kinetic energy from inertial layer:

$$\xi_r = \begin{cases} \xi_0, r < r_s - \frac{\Delta}{2} \\ \xi_0[1 - (r - r_s)/\Delta], r_s - \frac{\Delta}{2} < r < r_s + \frac{\Delta}{2} \\ 0, r_s + \frac{\Delta}{2} < r < a \end{cases} \text{and} \frac{d\xi_r}{dr} = \begin{cases} 0, r < r_s - \frac{\Delta}{2} \\ -\frac{\xi_0}{\Delta}, r_s - \frac{\Delta}{2} < r < r_s + \frac{\Delta}{2} \\ 0, r_s + \frac{\Delta}{2} < r < a \end{cases}. \tag{A12}$$

Therefore, by substituting Eq. (A12) into Eq. (A8), the modified inertial term, Eq. (A8) is then reduced as follows:

$$\begin{aligned}
\delta I &= -\frac{\pi\rho_0\omega_1\xi_0^2}{\Delta^2}\int_{r_s-\Delta/2}^{r_s+\Delta/2} drf(r)\left(\omega_1 + \Omega_0 g(r) - \frac{\Omega_0^2}{\omega_1}\frac{y}{2}\frac{g^4(r)}{u(r)}\right)r^3 \\
&\quad + \pi\rho_0\omega_1\frac{\xi_0^2}{\Delta}\int_{r_s-\Delta/2}^{r_s+\Delta/2} drf(r)\left(2\Omega_0 g(r) - \frac{\Omega_0^2}{\omega_1}y\frac{g^4(r)}{u(r)}\right)r^2 - \xi_0^2\frac{\pi\rho_0\omega_1}{2}\int_0^{r_s} rdr \\
&\quad \times \left(4\Omega_0 f(r)g(r) - \frac{\Omega_0^2}{\omega_1}rg^2(r)\frac{df(r)}{dr} - \frac{\Omega_0^2}{\omega_1}yg^2(r)\frac{d}{dr}\frac{f(r)g^2(r)r}{u(r)} - \frac{2\Omega_0^2}{\omega_1}y\frac{f(r)g^4(r)}{u(r)}\right) \\
&= -\frac{\pi\rho_0\omega_1\xi_0^2}{\Delta^2}\left(\omega_1 + \Omega_0 g_1 - \frac{\Omega_0^2}{\omega_1}\frac{yg_1^4}{2u_1}\right)f_1\int_{-\Delta/2}^{+\Delta/2} dx(r_s + x)^3 \\
&\quad + \pi\rho_0\omega_1\frac{\xi_0^2}{\Delta}\left(2\Omega_0 g_1 - \frac{\Omega_0^2}{\omega_1}\frac{yg_1^4}{u_1}\right)f_1\int_{-\Delta/2}^{+\Delta/2} dx(r_s + x)^2 - 2\pi\rho_0\omega_1\Omega_0 r_s^2\xi_0^2\int_0^1 \hat{r}d\hat{r}f(\hat{r})g(\hat{r}) \\
&\quad + \xi_0^2\frac{\pi\rho_0\omega_1 r_s^2}{2}\frac{\Omega_0^2}{\omega_1}\int_0^1 \hat{r}d\hat{r}\left(\hat{r}g^2(\hat{r})\frac{df(\hat{r})}{d\hat{r}} + yg^2(r)\frac{d}{d\hat{r}}\frac{f(\hat{r})g^2(\hat{r})\hat{r}}{u(\hat{r})} + 2y\frac{f(\hat{r})g^4(\hat{r})}{u(\hat{r})}\right) \\
&= -\frac{\pi\rho_0\omega_1\xi_0^2 r_s^3}{\Delta}\left(\omega_1 + \Omega_0 g_1 - \frac{\Omega_0^2}{\omega_1}\frac{yg_1^4}{2u_1}\right)f_1 + \pi\rho_0\omega_1\xi_0^2 r_s^2\left(2\Omega_0 g_1 - \frac{\Omega_0^2}{\omega_1}\frac{yg_1^4}{u_1}\right)f_1 - 2\pi\rho_0\xi_0^2 r_s^2\Omega_0\omega_1 \\
&\quad \times \int_0^1 \hat{r}d\hat{r}f(\hat{r})g(\hat{r}) + \xi_0^2\frac{\pi\rho_0\omega_1 r_s^2}{2}\frac{\Omega_0^2}{\omega_1}\int_0^1 \hat{r}d\hat{r}\left(\hat{r}g^2(\hat{r})\frac{df(\hat{r})}{d\hat{r}} + yg^2(r)\frac{d}{d\hat{r}}\frac{f(\hat{r})g^2(\hat{r})\hat{r}}{u(\hat{r})} + 2y\frac{f(\hat{r})g^4(\hat{r})}{u(\hat{r})}\right) \\
&= -\frac{\pi\rho_0\omega_1\xi_0^2 r_s^3}{\Delta}\omega_1\left(1 + \frac{g_1\Omega_0}{\omega_1} - \frac{\Omega_0^2}{\omega_1^2}\frac{yg_1^4}{2u_1}\right)f_1 + \pi\rho_0\xi_0^2 r_s^2\omega_1\Omega_0\left(C_1 + \frac{C_2\Omega_0}{\omega_1} - \frac{yg_1^4\Omega_0}{u_1\omega_1}\right)f_1.
\end{aligned} \tag{A13}$$

By substituting Δ into Eq. (A13), the normalized inertial term can be rewritten as

$$\delta\hat{I} = \left[-i\frac{\omega_1}{\omega_A}\left(1 + \frac{\Omega_0 g_1}{\omega_1} - \frac{yg_1^4}{2u_1}\frac{\Omega_0^2}{\omega_1^2}\right) + \frac{\omega_1\Omega_0}{\omega_A^2\hat{s}^2}\left(C_1 + \frac{C_2\Omega_0}{\omega_1} - \frac{yg_1^4}{u_1}\frac{\Omega_0}{\omega_1}\right)\right]f_1, \tag{A14}$$

with $y = \frac{m_i\Omega_0^2 R_0^2}{2kT_0}$. In general, the additional pressure generated by plasma rotation is much less than plasma pressure in tokamak plasmas, and thus we can neglect the terms with y in Eq. (A14) which is the modified inertial term for monotonic q profile. However, for the nonmonotonic safety factor profile, $q(r)$ should be expanded to the second order in r (or x) due to $q'(r_s) = 0$. Equation (A9) can be then rewritten as follows:

$$\frac{d}{dx}\left\{\left[3\omega^2 - \left(\frac{V_A}{R_0}(\delta q + q''_s x^2/2)\right)^2\right]\frac{d\xi_r}{dx}\right\} = 0, \tag{A15}$$

the solution of Eq. (A15) is

$$\xi_r = \frac{\xi_0}{2}\left[1 - \frac{2}{\pi}\frac{\Delta_+}{\Delta_+ + i\Delta_-}arctg\left(\frac{x}{\Delta_-}\right) - \frac{1}{\pi}\frac{\Delta_-}{\Delta_+ + i\Delta_-}\ln\frac{1 + x/\Delta_+}{1 - x/\Delta_+}\right], \tag{A16}$$

with $\Delta_- = \frac{1}{i}\sqrt{\frac{2(\sqrt{3}R_0\omega - \delta q V_A)}{q''_s V_A}}$ and $\Delta_+ = \frac{1}{i}\sqrt{\frac{2(\sqrt{3}R_0\omega + \delta q V_A)}{q''_s V_A}}$. It is easy to see that in Eq. (A16), the radial displacement ξ_r goes to ξ_0 (or zero) when x goes to $-\infty$ (or $+\infty$), thus Eq. (A16) is also a steplike function and can be taken the form of Eq. (A12).

However, the derivatives of ξ_r at the location of minimum q value (i.e., $x = 0$) is different and can be written as

$$\left.\frac{d\xi_r}{dr}\right|_{r=r_s} = -\frac{\xi_0}{\pi}\frac{\Delta_+ - i\Delta_-}{\Delta_+\Delta_-}. \tag{A17}$$

By substituting $\xi_r = \xi_0$ and Eq. (A17) into Eq. (A8), the normalized inertial term under the condition of nonmonotonic safety factor profile can be written as

$$\delta\hat{I} = \left[-i\frac{\omega_1}{\sqrt{2}\hat{s}\omega_A^2}\frac{\omega_+ - i\omega_-}{\omega_+\omega_-}\left(1 + \frac{g_1\Omega_0}{\omega_1}\right) + \frac{\Omega_0}{\hat{s}^2\omega_A^2}(C_1\omega_1 + C_2\Omega_0)\right]f_1, \tag{A18}$$

where $\hat{s} = r_s q_s''$.

[1] K. McGuire *et al.*, Phys. Rev. Lett. **50**, 891 (1983).
[2] L. Chen and M. N. Rosenbluth, Phys. Rev. Lett. **52**, 1122 (1984).
[3] R. B. White *et al.*, Phys. Rev. Lett. **60**, 2038 (1988).
[4] B. Coppi and F. Porcelli, Phys. Rev. Lett. **57**, 2272 (1986).
[5] W. W. Heidbrink *et al.*, Phys. Rev. Lett. **57**, 835 (1986).
[6] I. T. Chapman *et al.*, Nucl. Fusion **50**, 045007 (2010).
[7] I. T. Chapman *et al.*, Nucl. Fusion **51**, 073040 (2011).
[8] M.-D. Hua *et al.*, Plasma Phys. Control. Fusion **52**, 035009 (2010).
[9] L. Yu *et al.*, J. Phys. Soc. Jpn. **86**, 024501 (2017).
[10] J. P. Graves *et al.*, Plasma Phys. Control. Fusion **55**, 014005 (2013).
[11] J. E. Menard *et al.*, Nucl. Fusion **45**, 539 (2005).
[12] W. Deng *et al.*, Nucl. Fusion **54**, 013010 (2014).
[13] L. Yu *et al.*, Nucl. Fusion **57**, 036023 (2017).
[14] W. Chen *et al.*, Nucl. Fusion **50**, 084008 (2010).
[15] D. Pfefferle *et al.*, Nucl. Fusion **54**, 064020 (2014).
[16] M. Cecconello *et al.*, Plasma Phys. Control. Fusion **57**, 014006 (2015).
[17] F. Wang *et al.*, Phys. Plasmas **20**, 102506 (2013).
[18] X. Q. Wang *et al.*, Nucl. Fusion **56**, 036024 (2016).
[19] W. Xie, Phys. Plasmas **27**, 092504 (2020).
[20] Y. Q. Liu *et al.*, Phys. Plasmas **15**, 112503 (2008).
[21] M. N. Bussac *et al.*, Phys. Rev. Lett. **35**, 1638 (1975).
[22] X. T. Ding *et al.*, Nucl. Fusion **53**, 043015 (2013).